

# Crack prediction in EB-PVD thermal barrier coatings based on the simulation of residual stresses

J W Chen<sup>1</sup>, Y Zhao<sup>1,2,3</sup>, S Liu<sup>1</sup>, Z Z Zhang<sup>1</sup> and J Ma<sup>1</sup>

<sup>1</sup> NDT Lab, Laser Institute of Shandong Academy of Sciences, LISADA, Jinan, China

<sup>2</sup> Centre of NDT Engineer and Technique in Shandong, Jinan, China

E-mail: yang.aisin.zhao@gmail.com

**Abstract.** Thermal barrier coatings systems (TBCs) are widely used in the field of aerospace. The durability and insulating ability of TBCs are highly dependent on the residual stresses of top coatings, thus the investigation of the residual stresses is helpful to understand the failure mechanisms of TBCs. The simulation of residual stresses evolution in electron beam physical vapor deposition (EB-PVD) TBCs is described in this work. The interface morphology of TBCs subjected to cyclic heating and cooling is observed using scanning electron microscope (SEM). An interface model of TBCs is established based on thermal elastic-plastic finite method. Residual stress distributions in TBCs are obtained to reflect the influence of interfacial roughness. Both experimental and simulation results show that it is feasible to predict the crack location by stress analysis, which is crucial to failure prediction.

## 1. Introduction

Thermal barrier coatings (TBC) are deposited on the surface of super alloy to protect the substrate, which can improve the thermal efficiency of engine more than 60% at 1600°C [1-4]. TBCs are widely used in the field of aerospace. The major failure form of TBCs is the ceramic layer fall off from the bond coat during service. When the ceramic layers fall off, the high temperature gas will corrode the substrate which may have catastrophic consequences [5]. Hence, the study on the TBCs' failure mechanism has an important significance.

TBCs usually consist of a super alloy substrate (S), a metal bond coating (BC), a thermal grown oxide (TGO) and a top ceramic coating (TC). At present, preparation methods of TBC are commonly electron beam-physical vapor deposition (EB-PVD) and air-plasma spray (APS) in industry production [6]. Compared to APS, the EB-PVD method has the characteristics of high cost and good spraying quality [7]. In addition, TBCs prepared by the two methods have different interfacial morphology between BC and TC.



Because of the mismatch of fast contraction of sprayed coating layer, thermal expansion and possible phase transition, the residual stresses of thermal barrier coatings will increase during the preparation [8-10]. Furthermore, the shape of TGO and parameters of each layer have great influences on the stresses of TBCs, due to the complex interaction among thermal, elastic, plastic, oxidation, creep, sintering and phase transition. By studying the stress evolution, it is possible to predict the crack initiation and growth. Thus, the study on the stress field is very meaningful to understand the failure mechanism of TBCs.

The residual stresses in TBCs prepared by APS have been investigated using theory and experiment methods [11-14]. The main objectives of the present work are to obtain the stress field of TBCs prepared by EB-PVD using finite element method and to predict the crack initiation and propagation based on the simulation.

## 2. Experiment

### 2.1. Specimens and heat treatment

TBCs were composed of a metal bond coating and a top ceramic coating deposited on a GH3030 super alloy substrate. The size of the substrate was  $\Phi 30 \times 4$  mm. The main component of the metal bond coating was a NiCoCrAlY alloy, and the thickness of BC layer was about 120  $\mu$ m. On top of the bond coating, a ZrO<sub>2</sub>-7wt%Y<sub>2</sub>O<sub>3</sub> top coating with the thickness of 120  $\mu$ m was deposited. During the coating deposition using EB-PVD method, the TBCs were cooled from the preparation temperature of 850°C (the initial stress was zero) to room temperature (20°C). After the coating deposition, the specimens were subjected to thermal cycle treatments in a furnace. A single thermal cycle included three stages: the specimens were heated up to 1000°C in 10mins, kept at 1000°C for 1h, and cooled down the specimens to room temperature in 10mins at last. There were 5 groups of samples, and the number of thermal cycles was 0, 1, 10, 50 and 100h, respectively.

### 2.2. Microstructure

After the isothermal cycling treatments, the TBCs samples are cut into four equal parts along two diameters. The cross-sections are polished and then corroded using HCl(20ml) + CuSO<sub>4</sub>(5g) + H<sub>2</sub>O(100ml). Figure 1 indicates the scanning electron microscopy (SEM) results of TBCs on cross sections. It is shown that the TBCs consist of three layers. It is known that there is almost no TGO without oxidation treatment. After isothermal cycling treatments for 100h, a TGO layer related to the oxygen ingress through the porous TC layer and outward diffusion of Al in the BC layer is formed between the TC and BC layer.

More than 20 equidistant points distributed along the BC/TC interface were selected to measure the TGO thickness perpendicular to the interface. The thickness of TGO as a function of thermal cycle time is expressed by the power law equation below [15-16]

$$h^2 = k_p \times t \quad (1)$$

where  $h$  represents the thickness of TGO,  $t$  represents the holding time at high temperature, and  $k_p$  represents a regression constant, which is relevant to the porosity and thickness of TBC. Based on the experimental results,  $k_p$  equals to about 0.053  $\mu$ m<sup>2</sup>/h. By comparison with the results ( $\sim 0.17 \mu$ m<sup>2</sup>/h) of Zhu [17], the growth rate of TGO thickness prepared by EB-PVD is slower than that by APS. TC layer

begins to fall off when the thickness of TGO is greater than 8-10 $\mu\text{m}$  [18]. Therefore, TBCs prepared by EB-PVD have longer service life.

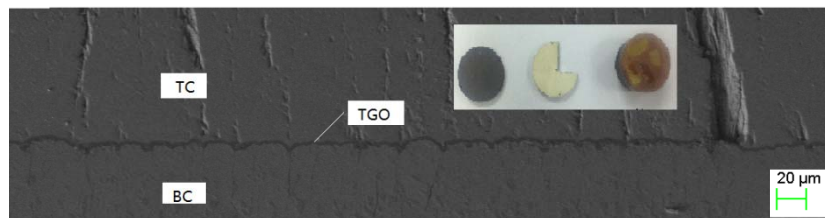


**Figure 1.** SEM images of TBCs after isothermal cycling treatments for 100h.

### 3. Finite element model

As illustrated in Figure 2, the simulation model corresponding to the scanning electron microscopy patterns in Figure 1 is shown. The model is composed of a TC, a TGO and a BC. The thickness of BC and TC are both 120 $\mu\text{m}$ . The thickness of TGO ranges from 0 to 10 $\mu\text{m}$ . The model is simulated using the finite element software ANSYS, and an axisymmetric analysis based on the coupled thermal and structure element PLANE 13 is used to reduce the data processing time.

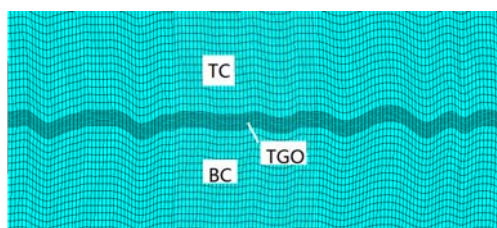


**Figure 2.** The finite element model corresponds to the scanning electron microscopy patterns.

Based on the experimental process, the temperature of isothermal cycling is loaded on the TBCs. The temperature load of one thermal cycle is composed of a heating process from 20 to 1000 $^{\circ}\text{C}$  for 10mins, a holding process at 1000 $^{\circ}\text{C}$  for 1h and a cooling process from 1000 to 20 $^{\circ}\text{C}$  for 10 mins.

**Table 1.** Material property parameters [11, 19].

|    | T( $^{\circ}\text{C}$ ) | E(GPa) | $\nu$ | $\alpha_{\text{px}}(10^{-6}/^{\circ}\text{C})$ | $\rho$ ( $\text{kgm}^{-3}$ ) | $k(\text{Wm}^{-1}\text{K}^{-1})$ | $C(\text{Jkg}^{-1}\text{K}^{-1})$ | $\sigma_{\text{Y}}(\text{MPa})$ |
|----|-------------------------|--------|-------|--|------------------------------|----------------------------------|-----------------------------------|---------------------------------|
| S  | 20                      | 220    |       | 14.8   |                              |                                  |                                   |                                 |
|    | 600                     | 170    | 0.33  | 16.9   | 7900                         | 16.3                             | 437                               |                                 |
|    | 1100                    | 120    |       | 18   |                              |                                  |                                   |                                 |
| BC | 20                      | 200    |       | 13.2   |                              |                                  |                                   | 400                             |
|    | 600                     | 160    | 0.31  | 15.2   | 7320                         | 16.1                             | 501                               | 300                             |
|    | 1100                    | 110    |       | 17.6   |                              |                                  |                                   | 50                              |
| TG |                         | 360    | 0.27  | 8  | 3980                         | 30                               | 800                               |                                 |
|    | 20                      | 48     |       | 9  |                              |                                  |                                   |                                 |
| TC | 600                     | 40     | 0.11  | 10.1   | 5600                         | 1.8                              | 500                               |                                 |
|    | 1100                    | 22     |       | 12.2   |                              |                                  |                                   |                                 |

In this work, it is assumed that the TC and TGO are elastic materials and the BC is an elastic-plastic material with temperature dependence of yield strength. The property parameters are shown in Table 1. The thermal load is agreement with the experimental situation. And just one cycle process is simulated because the creep characteristic is not taken into account.

#### 4. Results and discussion

Compared with the mode II fracture resulted from shear stress component  $\sigma_{xy}$ , the normal stress components  $\sigma_x$  and  $\sigma_y$  more likely lead to the mode I fracture [20]. The component  $\sigma_x$  is a cause of a vertical surface crack, while  $\sigma_y$  can be used to predict the crack initiation and propagation along the BC/TC interfaces.

##### 4.1. Effect of interfacial roughness

The stress field of the BC and TC layers in the x direction with different interfacial roughness is shown in Figures 3 and 4. The results are parts of the interface in Figure 1. As shown in Figure 3, the maximum value of tensile stress occurs at the peak region and the maximum compressive stress lies in the valley region. By comparing Figures 3(a), (b) and (c), it is shown that the stress levels are dependent on the curvature of the interface. The maximum compressive stress at the valley increases with the increase of curvature. The stress in the valley ranges from -116Mpa to -341Mpa and the stress at the peak ranges from -71.4Mpa to 63.5Mpa. Therefore, the tension stress at the peak may cause the generation of vertical surface cracks, and the probability of crack generation increases with the increase of curvature.

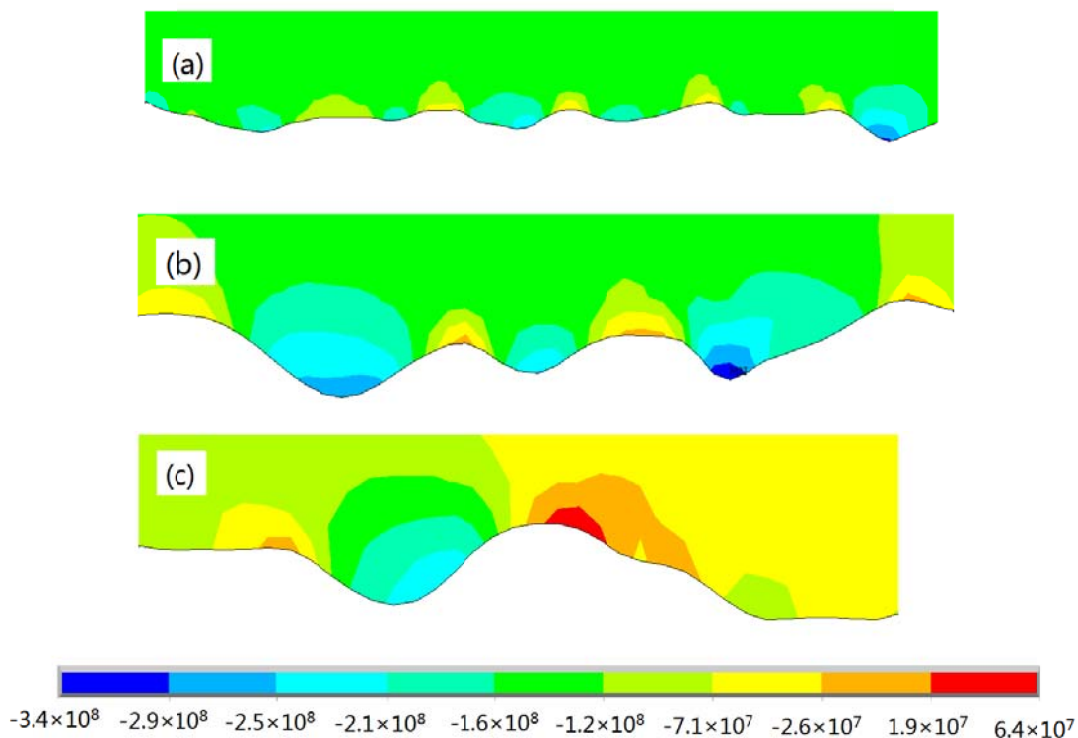


**Figure 3.** The contour plot of  $\sigma_x$  at the TC layer after cooling.

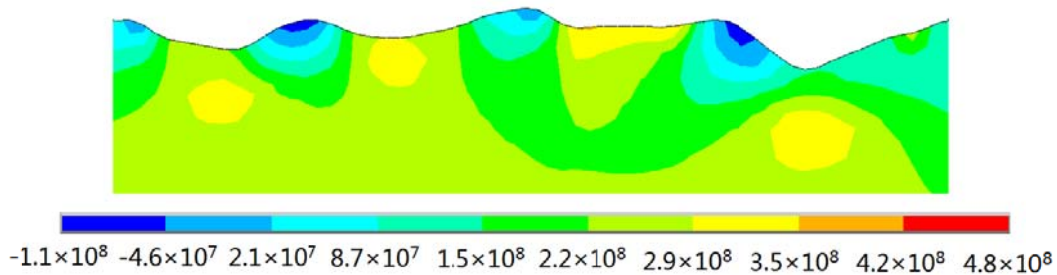


**Figure 4.** The contour plot of  $\sigma_x$  at the BC layer after cooling.

As shown in Figure 4, contrary to the stress distribution in TC layer, the maximum value of tension stress occurs at the valley region and the maximum compressive stress lies in the peak region. The stress level also increases with the increase of curvature. The maximum tension stress in the valley ranges from 153Mpa to 484Mpa. Therefore, the vertical surface cracks are most likely to initiate at the valley.

The stress contours of the BC and TC layers in the y direction with different interfacial roughness are shown in Figure 5. It is shown that the maximum tensile stress occurs at the valley region and the maximum compressive stress lies in the peak region at the TC layer, and the regulation is contrary at the BC layer. The maximum tension stresses at the TC and BC layers are 123Mpa and 484Mpa, respectively. Consequently, the cracks in the TBCs start at the valley of TC layer and at the peak of BC layer.

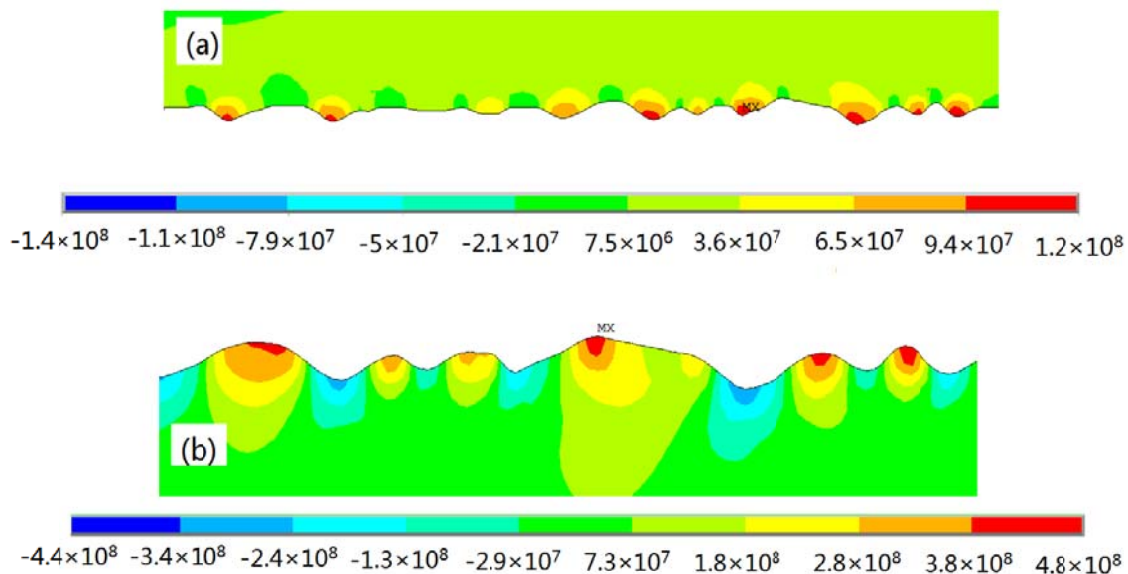


**Figure 5.** The contour plot of  $\sigma_y$  after cooling (a) at the TC layer and (b) at the BC layer.

#### 4.2. Crack prediction

In view of the stress analyses on the TC/BC interface, the vertical surface cracks at the TC and BC layer occur at the peak and valley, respectively. This is consistent with the experimental results shown in Figure 6. Figure 6(a) contains two cracks: one located at the peak (in the TC layer) and the other

located at the valley (in the BC layer). All the cracks are located at the valley in the BC layer as shown in Figure 6(b).

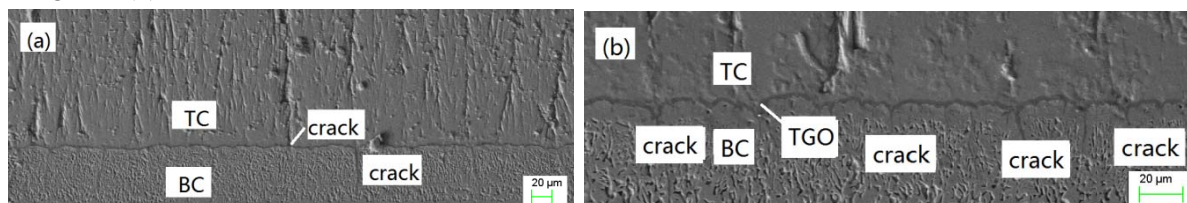


**Figure 6.** SEM of an EB-PVD TBCs after isothermal cycling treatments for (a)50h and (b)100h.

The crack in Figure 7(a) originates from the interface between TC and TGO, and extends into the TC layer along the lateral direction. The crack in Figure 7(b) originates from the interface between BC and TGO, and extends along the interface. It is hard to tell the initial position of both the cracks. Based on the analyses above, it can be predicted that the cracks in Figure 7(a) and (b) occurs at the valley (in the TC layer) and peak (in the BC layer), respectively.

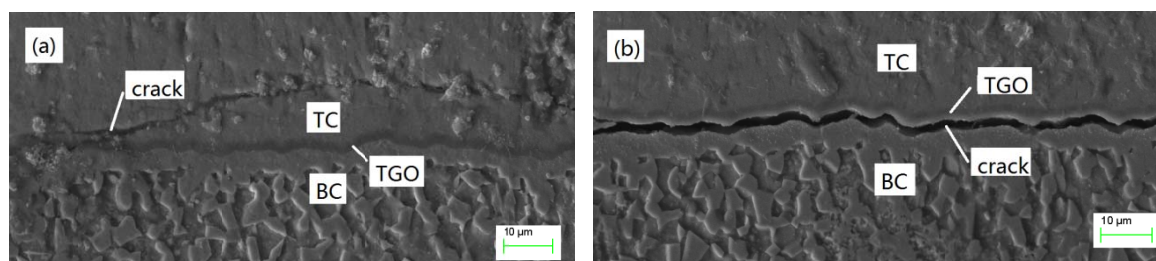


**Figure 7.** SEM of an EB-PVD TBCs after isothermal cycling treatments for 100h.

## 5. Conclusions

In this work, the finite element method based on thermal elastic-plastic has been used to establish interface model of TBC. Then, we have calculated the residual stress field of EB-PVD TBC to analysis the influence of interface morphology on residual stress. The influence of interface morphology on residual stress is analyzed via the calculation of the residual stress field of EB-PVD TBC enduring cycle heating and cooling. The main conclusions are summarized as follows:

(1) In the TC layer, it is more likely to be in the state of tension stress at the peak, which may result in the generation of vertical surface cracks. And the probability of crack generation increases with the increase of curvature. In the BC layer, the initiation of vertical surface cracks is most likely to occur at the valley. In addition, the crack path at TC/BC interfaces and separation of the TBC layers are more likely to start at the valley of TC layer and at the peak of BC layer.

(2) By comparing the experimental and simulation results, it is feasible to predict the crack location by stress analysis. Therefore, the simulation of residual stresses evolution is valuable for studying the failure mechanism of TBCs.

## Acknowledgments

This work has been supported by the National Natural Science Foundation of China (No. 51205240), the Outstanding Young Scientists Program of Shandong Academy of Sciences (No. 201505) and Independent Innovation Projects of Jinan (No. 201407).

## References

- [1] Zhao Y, Chen J and Zhang Z 2015 *Opt. Eng* **54** 094104
- [2] Miller R 1987 *Surf. Coat. Technol* **30** 1
- [3] Meier S and Gupta D 1994 *J. Eng. Gas Turb. Power* **116** 250
- [4] Miller R 1997 *J. Therm. Spray Technol* **6** 35
- [5] Pature N, Gell M and Jordan E 2002 *Science* **296** 280
- [6] Chen D and Gell M 2007 *J. Amer. Chem. Soc* **90** 3160
- [7] Schulz U and Fritstcher K 1997 *Mater. Sci. Forum* **957** 251
- [8] Wenzelburger M, Escribano M and Gadow R 2004 *Surf. Coat. Technol* **180-181** 429
- [9] Zhang X, Xu B and Wang H 2005 *Thin Solid Films* **488** 274
- [10] Yang L, Liu Q, Zhou Y, Mao W and Lu C 2013 *J. Mater. Sci. Technol* **30** 371
- [11] Mao W, Chen Q, Dai C, Yang L, Zhou Y C and Lu C 2010 *Surf. Coat. Technol* **204** 3573
- [12] Song M, Ma Y and Gong S 2011 *Prog. Nat. Sci* **21** 262
- [13] Mao W, Jiang J, Zhou Y and Lu C 2011 *Surf. Coat. Technol* **205** 3093
- [14] Ranjbar-Far M, Absi J, Mariaux G and Dubois F 2010 *Mater. Des* **31** 772
- [15] Rosler J, Baker M and Aufzug K 2004 *Acta Mater* **52** 4809
- [16] Ranjbar-Far M, Absi J, Mariaux G and Dubois F 2010 *Mater. Des* **31** 772
- [17] Zhu J, Chen W and Xie H 2015 *Sci. China Phys. Mech. Astr* **58** 1
- [18] Hernandez M, Karlsson A and Bartsch M 2009 *Surf. Coat. Technol* **203** 3549
- [19] Wang Q, Jiang J and Mao W 2010 *Mater. Rev* **24** 259
- [20] Ranjbar-Far M, Absi J and Mariaux G 2012 *J. Therm. Spray Technol* **21** 1234